Effects of Substituted Side-Chain Position on Donor–Acceptor Conjugated Copolymers

SANG KYU LEE,[1] SHINUK CHO,[2] MINGHONG TONG,[3] JUNG HWA SEO,[3] ALAN J. HEEGER[3]

[1]Energy Materials Research Center, Korea Research Institute of Chemical Technology (KRICT), Daejeon 305-600, South Korea

[2]Department of Physics and EHSRC, University of Ulsan, Ulsan 680-749, South Korea

[3]Center for Polymers and Organic Solids, University of California at Santa Barbara, Santa Barbara, California 93106-5090

Received 16 November 2010; accepted 25 January 2011
DOI: 10.1002/pola.24607
Published online 1 March 2011 in Wiley Online Library (wileyonlinelibrary.com).

ABSTRACT: The optical properties and electrical properties of a series of low-band-gap conjugated copolymers, in which alkyl side chains were substituted at various positions, were investigated using donor–acceptor conjugated copolymers consisting of a cyclopentadithiophene derivative and dithienyl-benzothiadiazole. With substituted side chains, the intrinsic properties of the copolymers were significantly altered by perturbations of the intramolecular charge transfer. The absorption of poly[2,6-(4,4-bis(2-octyl)-4*H*-cyclopenta-[2,1-b:3,4-b′]dithiophene)-*alt*-4,7-bis(4-octyl-thiophene-2-yl)benzo-2,1,3-thiadiazole] [**PCPDT-ttOTBTOT** (**P2**)], which assumed a tail–tail configuration, tended to blue shift relative to the absorption of poly[2,6-(4,4-bis(2-octyl)-4*H*-cyclopenta-[2,1-b:3,4-b′]dithiophene)-*alt*-4,7-bis(thiophene-2-yl)benzo-2,1,3-thiadiazole] [**PCPDT-TBTT** (**P1**)]. The absorption of poly[2,6-(4,4-bis(2-octyl)-4*H*-cyclopenta-[2,1-b:3,4-b′]dithiophene)-*alt*-4,7-bis(3-octyl-thiophene-2-yl)benzo-2,1,3-thiadiazole] [**PCPDT-hhOTBTOT** (**P3**)], which assumed a head–head configuration, was blue shifted relative to that of **P2**. The electrical transport properties of field-effect transistors were sensitive to the side chain position. The field-effect mobility in **P2** ($\mu_2 = 1.8 \times 10^{-3}$ cm^2/V s) was slightly lower than that in **P1** ($\mu_1 = 4.9 \times 10^{-3}$ cm^2/V s). However, the mobility of **P3** was very low ($\mu_3 = 3.8 \times 10^{-6}$ cm^2/V s). Photoexcitation spectroscopy showed that the charge generation efficiency (shown in transient absorption spectra) and polaron pair mobility in **P1** and **P2** were higher than in **P3**, yielding **P1** and **P2** device performances that were better than the performance of devices based on **P3**. © 2011 Wiley Periodicals, Inc. J Polym Sci Part A: Polym Chem 49: 1821–1829, 2011

KEYWORDS: conjugated polymers; donor–acceptor copolymers; photophysics; polymer field-effect transistors; side-chain effect; thin film

INTRODUCTION Because of the low band-gap property together with relatively high hole mobilities, conjugated copolymers containing electron donor–acceptor (D–A) repeating units have drawn considerable attention for use as active materials in organic electronic devices, such as bulk heterojunction photovoltaic cells and polymer field-effect transistors (FETs).[1–5] Most polymer electronic devices are fabricated by solution processing, which represents an attractive advantage of polymer electronics over their inorganic counterparts. Although the conjugated core units of D–A conjugated copolymers convey solubility, D–A copolymers have relatively low solubility if they have a high molecular weight (M_w). Because the best performances have usually been obtained using high M_w materials,[6,7] achieving high M_w with good solubility is anticipated to be an important goal for achieving high performance polymer electronic devices.

As a simple way to improve the solubility of high M_w D–A copolymers, alkyl or alkoxy side chains may be introduced at the thiophene unit. However, substitution of side chains in conventional conjugated polymers often alters the configuration of the conjugated chain, thereby affecting the electronic properties. Consequently, the polymers display properties that differ compared with the original analogs.[8,9] Such side chain effects can critically affect the electronic properties of D–A conjugated copolymers because significant alterations of the main chain configuration may interrupt intramolecular charge transfer (ICT), which is the driving force for the low band-gap properties of D–A conjugated copolymers.

In a previous report, we described the effects of several substituted side chains (alkyl or alkoxy) on the optical and electrical properties of D–A conjugated copolymers.[10] The substituted alkyl or alkoxy side chains significantly altered the optical properties and electrical properties of D–A conjugated copolymers due to steric hindrance. In this study, we investigated the effects of the position of substituted side chains (alkyl) on the optical properties and electrical properties of D–A conjugated copolymers based on cyclopentadithiophene derivatives and dithienyl-benzothiadiazole (DTBT) as the donor and acceptor moieties, respectively.

Additional Supporting Information may be found in the online version of this article. Correspondence to: S. Cho (E-mail: sucho@ulsan.ac.kr)
Journal of Polymer Science Part A: Polymer Chemistry, Vol. 49, 1821–1829 (2011)

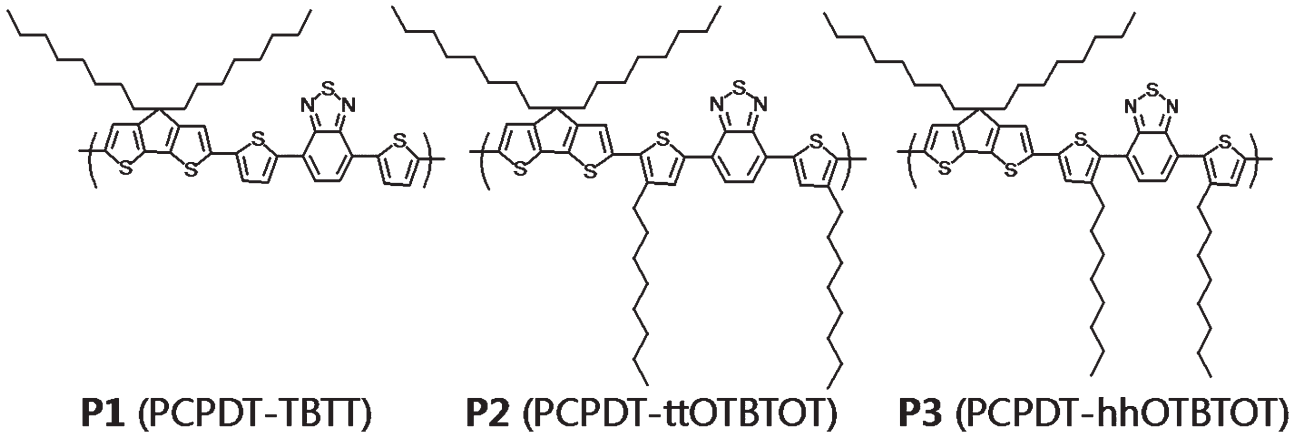

FIGURE 1 Chemical structures of **P1** (left), **P2** (middle), and **P3** (right).

RESULTS AND DISCUSSION

Chemical Structures

Figure 1 shows the chemical structures of the D–A conjugated copolymers studied in this work. Alkyl side chains were introduced at different positions in the original copolymer, poly[2,6-(4,4-bis(2-octyl)-4*H*-cyclopenta-[2,1-b:3,4-b′]dithiophene)-*alt*-4,7-bis(thiophene-2-yl)benzo-2,1,3-thiadiazole] (**PCPDT-TBTT**, **P1**), at the thiophene moiety of DTBT.[11] Alkyl chains were introduced in a tail–tail configuration into the copolymer poly[2,6-(4,4-bis(2-octyl)-4*H*-cyclopenta-[2,1-b:3,4-b′]dithiophene)-*alt*-4,7-bis(4-octyl-thiophene-2-yl)benzo-2,1,3-thiadiazole] (**PCPDT-ttOTBTOT**, **P2**), and alkyl chains were introduced in a head–head configuration into the copolymer poly[2,6-(4,4-bis(2-octyl)-4*H*-cyclopenta-[2,1-b:3,4-b′]dithiophene)-*alt*-4,7-bis(3-octyl-thiophene-2-yl)benzo-2,1,3-thiadiazole] (**PCPDT-hhOTBTOT**, **P3**). The synthetic details and chemical properties of these copolymers are described in the Supporting Information.

Steady-State Optical Properties

Substitution of side chains at different positions induced dramatic shifts in the absorption spectrum. Figure 2 shows the UV–Vis absorption spectra of **P1**, **P2**, and **P3** thin films. For **P2**, the onset of absorption was blue shifted by 40 nm compared with **P1**. In the case of **P3**, the onset of absorption was more blue shifted by 146 nm compared with **P1**. The absorption spectra of **P1** and **P2** were typical of D–A conjugated copolymer films (two distinct broad absorption peaks). However for **P3**, the two distinct main absorption peaks were not clearly separated. The short wavelength absorption peaks were attributed to a delocalized π–π^* transition in the polymer chains, and the long wavelength absorption peaks were attributed to a localized ICT between the D–A–D charge transfer states in the DTBT segment. The origin of the low band-gap properties in D–A conjugated copolymers is understood to be based on ICT between the donor and acceptor segments, and stronger ICT induces a red shift in the absorption spectra of D–A conjugated copolymers.[12–14] Therefore, the blue shifted absorption spectra for **P2** and **P3** may originate from weaker ICT. The spectral shift, in combination with a reduction in the relative intensity of the long wavelength absorption peaks relative to the short wavelength absorption peaks also indicated a weaker ICT for **P2** and **P3** compared with **P1**, and the ICT strength of **P3** was much weaker than that of **P2**.

Substitution of the side chains in D–A conjugated copolymers critically affected the properties of the copolymers beyond general side chain effects. Small alterations in the main chain configuration significantly interrupted the ICT, reducing the strength of the low-band-gap properties. Interestingly, substitution of alkoxy side chains at the same positions induced the opposite spectral shifts.[10]

Electronic Band Structures

Perturbation of the electronic band structures on substitution of side chains at various positions was examined by ultraviolet photoelectron spectroscopy (UPS) measurements of **P1**, **P2**, and **P3** thin films, as shown in Figure 3. The Fermi energy (E_F) was determined from the gold (Au) surface, and all other spectra were plotted with respect to this value. The normalized secondary edges of all films are shown in Figure 3(a). The vacuum levels (VLs) of the

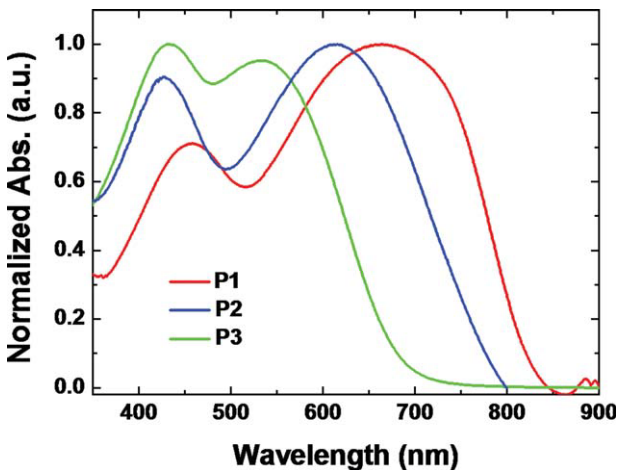

FIGURE 2 UV–Vis absorption spectra of **P1**, **P2**, and **P3**. [Color figure can be viewed in the online issue, which is available at wileyonlinelibrary.com.]

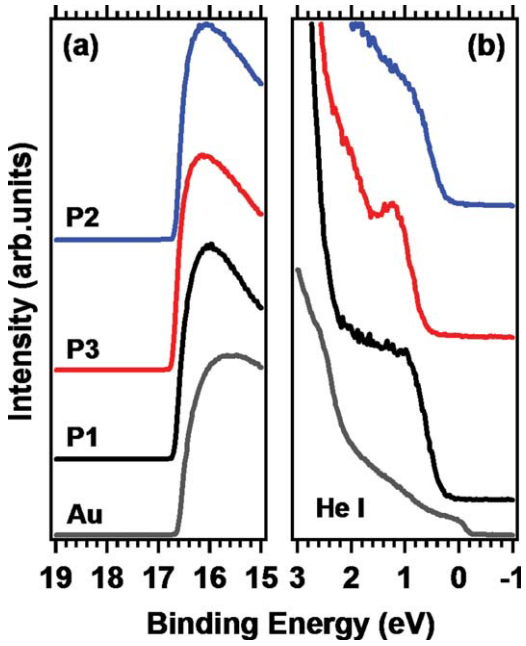

FIGURE 3 UPS spectra of **P1**, **P2**, and **P3**. The spectrum obtained from Au substrate is added for reference. [Color figure can be viewed in the online issue, which is available at wileyonlinelibrary.com.]

samples were determined by linear extrapolation of the secondary electron cutoffs on the high binding energy side of the UPS spectra (15–19 eV). The secondary edges shifted slightly to higher binding energies for each of **P1**, **P2**, and **P3** thin films compared with the edge of Au. A comparison of the three copolymers showed that the secondary edge of **P2** shifted less when compared with the edge of **P1**, whereas the secondary electron cutoffs of **P3** shifted toward a higher binding energy than that of **P1**. Because the VL shift indicated the magnitude of the interfacial dipole, the UPS spectra suggested that **P3** had a relatively strong interfacial dipole (the VL shift of **P3** was 0.11 eV) and **P2** had a relatively weak interfacial dipole (the VL shift of **P2** was 0.03 eV). The VL shift of the original copolymer, **P1**, was measured to be 0.06 eV.

Figure 3(b) shows the highest occupied molecular orbital (HOMO) onsets for **P1**, **P2**, and **P3**. Comparison of the shift in the HOMO onset to E_F for Au provided the relative position of the HOMO level. The ionization potential was determined using the incident photon energy ($h\nu$), the secondary cutoff, and the onset of the HOMO.[15] The ionization potential values determined for the polymers were 4.83 eV for **P1**, 4.77 eV for **P2**, and 5.07 eV for **P3**.

The energy level diagrams for **P1**, **P2**, and **P3**, as inferred from the UPS data, are illustrated in Figure 4. The values shown for each HOMO and lowest unoccupied molecular orbital (LUMO) indicate the energy difference with respect to E_F for Au. The energy differences between the E_F of Au and the HOMO of **P1**, **P2**, and **P3** were 0.32, 0.24, and 0.61 eV, respectively.

Electrical Properties Based on FETs

The effects of side chain substitution position on the electrical transport properties were examined by measuring the field-effect properties of each of the three copolymers. Figure 5 shows the transfer characteristics, I_{ds} versus V_{gs}, of the copolymer FETs fabricated using **P1**, **P2**, and **P3**.

The FET properties of the copolymers were significantly influenced by the side chain position. The FET mobilities were calculated in the saturation regime using the following equation: $I_{ds} = (W/2L)\mu C_i\ (V_{gs} - V_{th})$,[2] where W and L are the channel width and length, respectively, C_i is the capacitance per unit area of the insulation layer. Linear plots of $I_{ds}^{1/2}$ versus V_{gs}, deduced from the I_{ds} versus V_{gs} measurements, yielded hole mobilities of $\mu_1 = 4.9 \times 10^{-3}$ cm^2/V s, $\mu_2 = 1.8 \times 10^{-3}$ cm^2/V s, and $\mu_3 = 3.8 \times 10^{-6}$ cm^2/V s for **P1** (μ_1), **P2** (μ_2), and **P3** (μ_3), respectively. Details of the FET performance data, including mobilities, on/off ratios, and threshold voltages obtained from these polymers are listed in Table 1.

P1 and **P2** FETs showed good p-type FET performance with good output characteristics (Fig. 6). However for **P3**, the FET

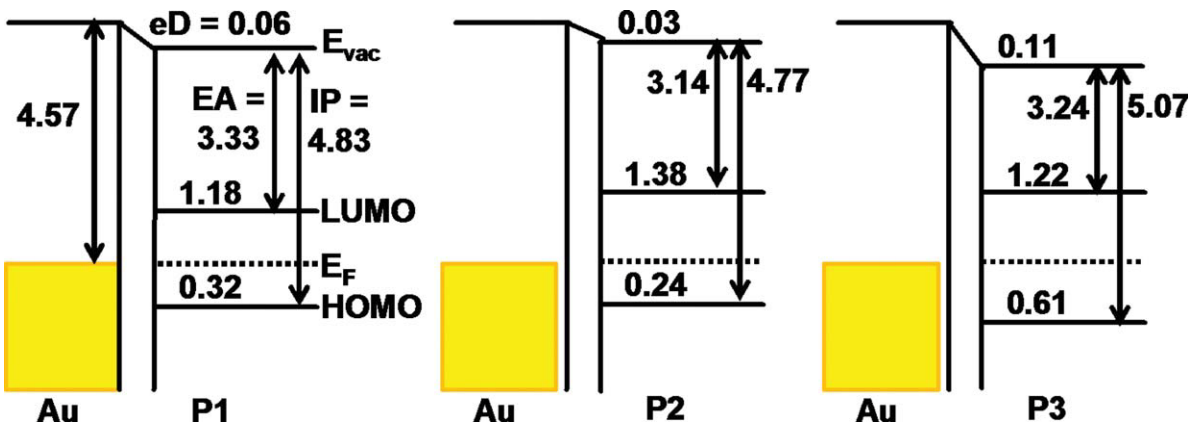

FIGURE 4 Energy level diagrams of **P1**, **P2**, and **P3** deduced from the UPS and UV–Vis spectra. [Color figure can be viewed in the online issue, which is available at wileyonlinelibrary.com.]

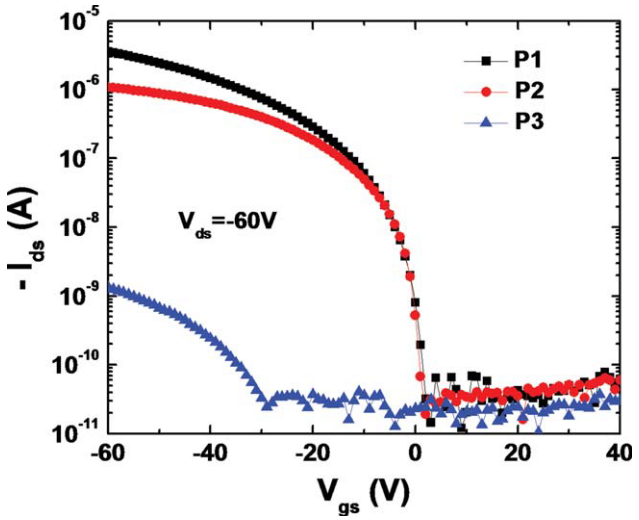

FIGURE 5 Transfer characteristics of **P1**, **P2**, and **P3** FETs. [Color figure can be viewed in the online issue, which is available at wileyonlinelibrary.com.]

performance was very poor. Moreover, the threshold voltage (V_{th}) obtained from the $I_{ds}^{1/2}$ versus V_{gs} curves was −28 V, indicating a relatively high density of charge carrier traps. Note that the highest mobility in each copolymer was obtained from postheat-treated devices. Figure 7 shows results from an examination of μ as a function of the annealing temperature.

M_w open plays an important role in determining the electronic properties of conjugated polymers. Increased mobility has been observed at high M_w in several instances. The number average molecular weight (M_n) of each polymer was 11,000 for **P1** (polydispersity index (PDI): 2.0), 9000 for **P2** (PDI: 1.3), and 12,000 for **P3** (PDI: 2.0). There was no big difference in M_n. Therefore, different electronic properties of **P1**, **P2**, and **P3** were not originated from the effect of M_w.

Thin Film Morphology

Slight modifications of the molecular structure open induced significant variations in the morphology, which significantly affected device performance. A morphological study of thin films of each of the three copolymers, measured by atomic force microscopy (AFM), however, did not provide a clear explanation for the differences between the FET properties of the three copolymers. Figure 8 shows tapping mode AFM

TABLE 1 Summary of the FET Properties and Postannealing Condition

	Mobility (cm^2/V s)	On/Off Ratio	V_T (V)	Optimized Annealing Condition (°C)
P1	4.9×10^{-3}	1×10^5	−3.5	200
P2	1.8×10^{-3}	3×10^4	0.5	175
P3	3.8×10^{-6}	5×10^1	−28	150

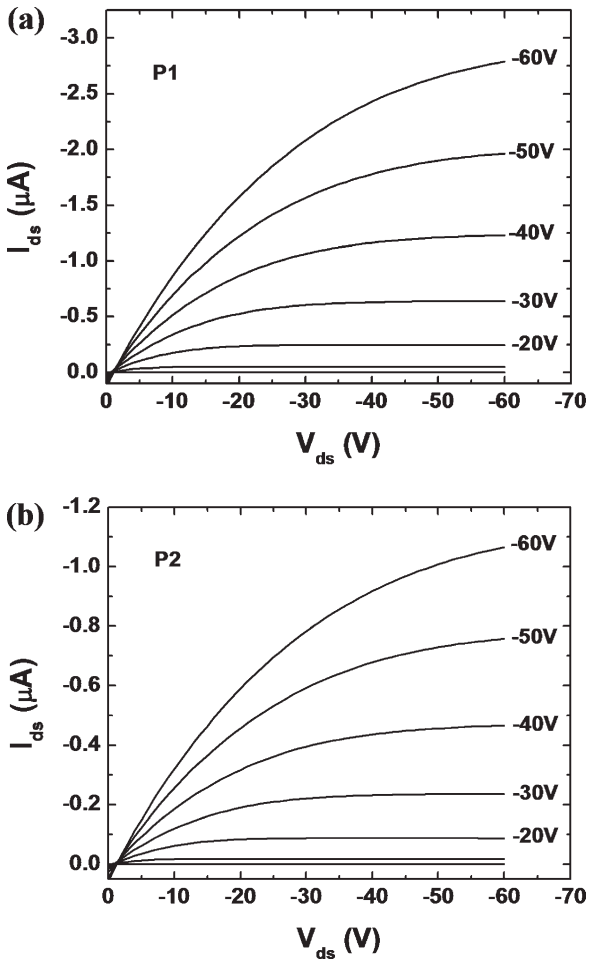

FIGURE 6 Output characteristics of (a) **P1** and (b) **P2** FETs.

images (2 × 2 μm^2 scan area) of **P1**, **P2**, and **P3** thin films deposited on Si/SiO_2 substrates. All AFM topographies exhibited a quite uniform film consisting of fine, regular grains. In

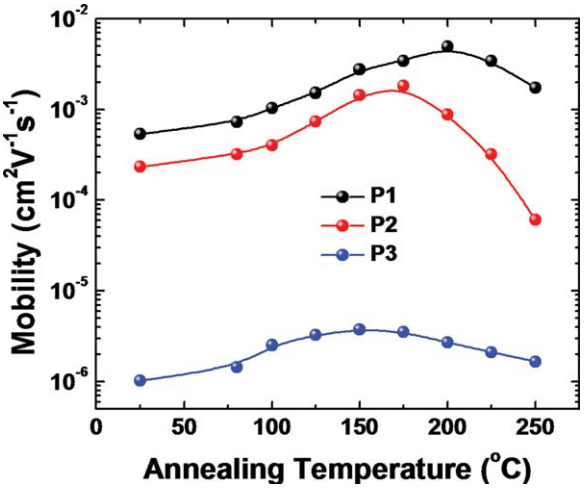

FIGURE 7 The postannealing temperature dependence of hole mobility. [Color figure can be viewed in the online issue, which is available at wileyonlinelibrary.com.]

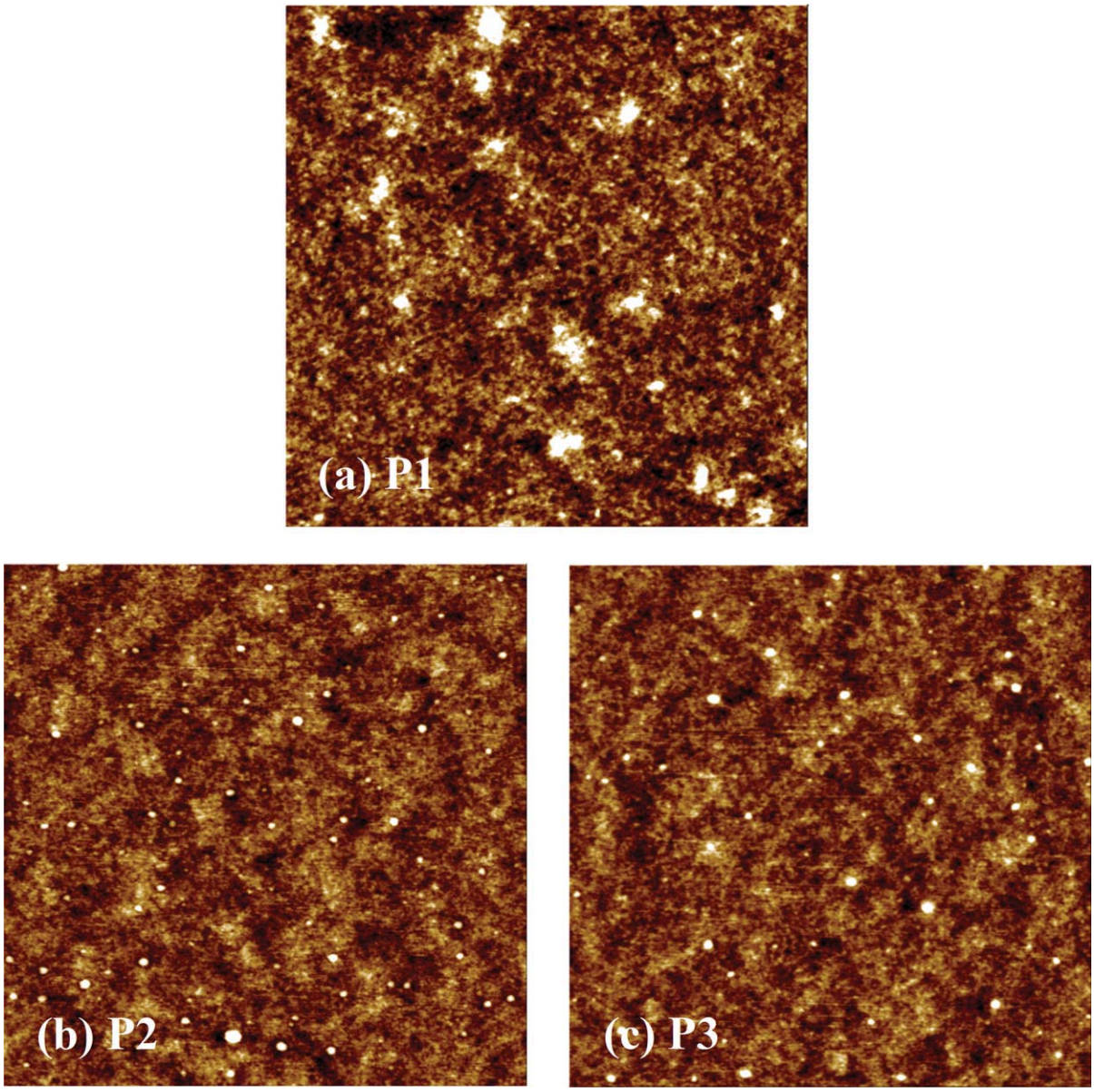

FIGURE 8 Surface morphology of **P1**, **P2**, and **P3** thin films. [Color figure can be viewed in the online issue, which is available at wileyonlinelibrary.com.]

addition, any intense reflection peaks were detected by X-ray diffraction (XRD) measurement. The morphological natures of all copolymers were simply amorphous (Supporting Information).

Quantum Chemical Calculations

The relatively high hole injection barrier (0.61 eV) between the Au electrode and the HOMO of **P3** may have been the reason underlying the low performance of the **P3** FET. However, considering that the barrier height was 0.31 eV for **P1**, the difference (decrease) in FET performance of **P3** was excessive relative to the difference in hole injection barrier. Although the hole injection barrier in **P2** was lower than in **P1**, a slightly lower performance for the **P2** FET when compared with the **P1** FET, was not expected.

The side chain effects were rationalized by assuming that steric hindrance due to side chain functionalization was the strongest influencing factor because it could alter the coplanarity of a conjugated backbone. Localization of the HOMO isosurface by physical chain distortion imposes the largest limitations on charge transport properties. The extent to which the side chains disturbed the main chain conformation was investigated by performing semiempirical quantum chemical simulations using the parameterized model 3 (PM3).

Figure 9 shows the charge-density isosurfaces for the HOMO and LUMO levels of **P1**, **P2**, and **P3** in the most energetically favorable geometry. The HOMO isosurface of **P1** [Fig. 9(a)] showed delocalization at both the donor and acceptor sites. The conjugated backbone was relatively flat. However, the

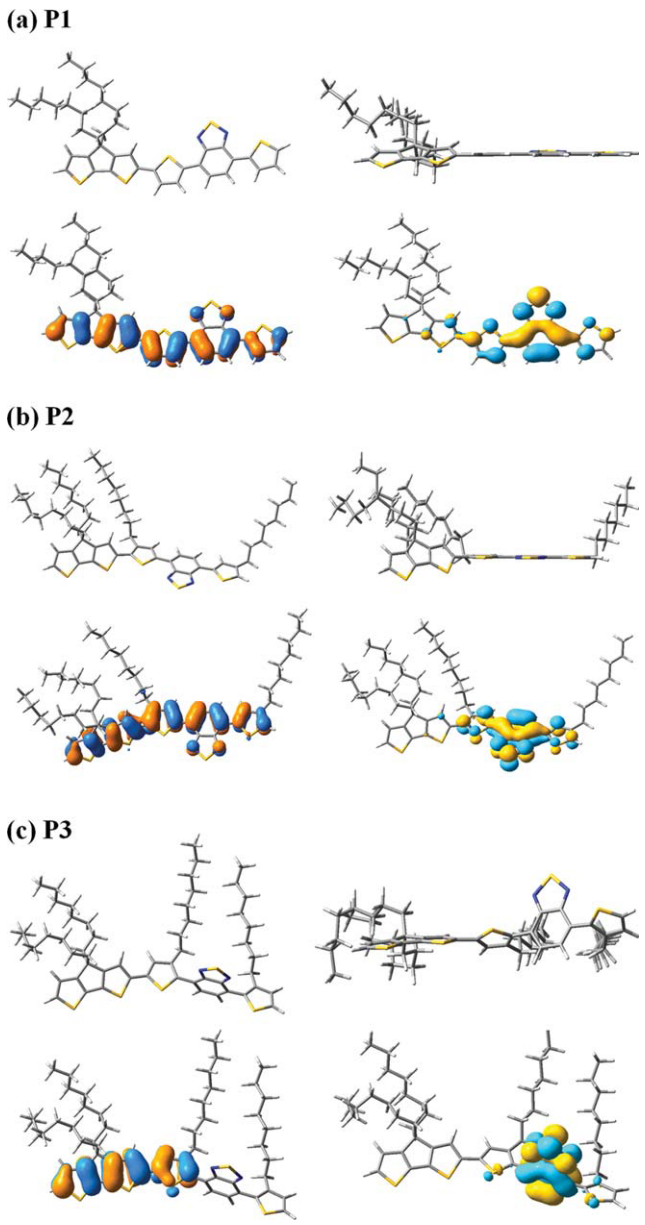

FIGURE 9 Energetically most favorable geometries and the HOMO and LUMO isosurfaces of **P1**, **P2**, and **P3**.

LUMO isosurface of **P1** tended to be localized on the benzothiadiazole. Although the HOMO and LUMO isosurface configurations of **P2** [Fig. 9(b)] were quite similar to those of **P1**, the backbone was slightly more distorted than that of **P1**. Thus, we attributed the slightly lower mobility of **P2** to the slightly worse planarity of the conjugated backbone. Strong steric hindrance by the alkyl side chains at the head–head positions in **P3** [Fig. 9(c)] dramatically twisted the structure of the conjugated backbone. Both the LUMO orbital and the HOMO orbital were localized, consistent with the lower values obtained for the hole mobility.

Excitation State Optical Properties

The characteristic photoexcitation properties of the three copolymer samples were studied using transient absorption (TA) spectroscopy. The TA spectra at three different time delays in the thin films of the three samples, **P1**, **P2**, and **P3**, are depicted in Figure 10. The pump beam from an optical parametric amplifier (OPA) was used to excite the low energy absorption band of the polymers. In all three samples, similar TA spectral features were observed: two photo-induced absorption (PA) bands (PA_1 and PA_2) and one photobleaching (PB) band, which overlapped with the spectral range of the ground state absorption of the samples. The PA_1 bands in the near-infrared (IR) in the three samples were assigned to singlet excited state absorption, a transition from the lowest singlet exciton to a higher energy state. The PA_2 band, which displayed a slower temporal evolution, was attributed to polaron and/or polaron pair absorption, which has been observed in other π-conjugated polymers and D–A copolymers.[16–18] The peak position of the PA_1 band for **P3** was located around 1000 nm, whereas the corresponding peaks for other two polymers (**P1** and **P2**) were longer than 1050 nm. The relative strength of the PA_2 band for the three polymers varied, with a stronger band for **P1**, a weaker band for **P2**, and a much smaller band for **P3**, indicating different polaron generation efficiencies in the samples.

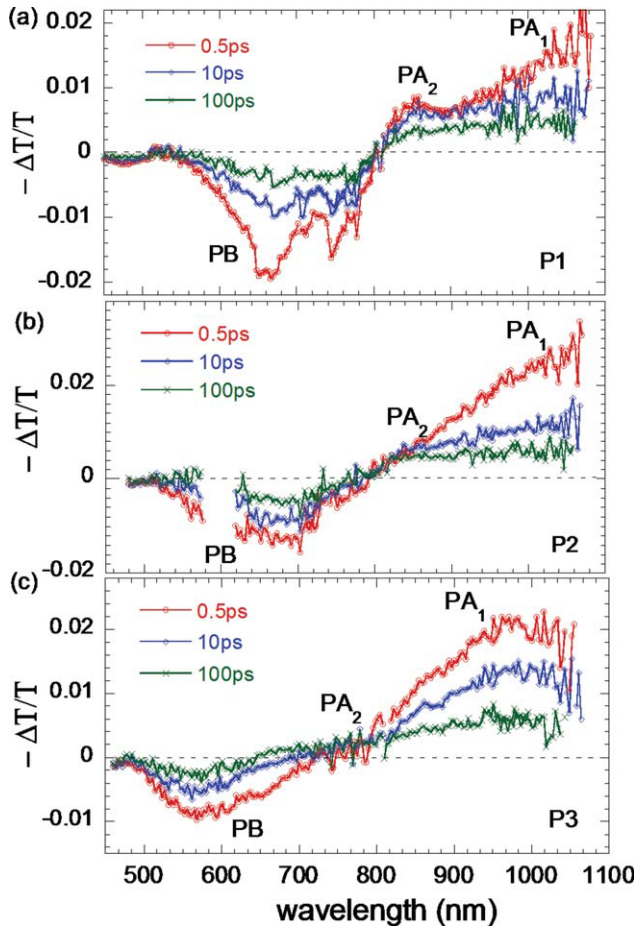

FIGURE 10 TA spectra at three different time delays in the thin films of **P1**, **P2**, and **P3**. [Color figure can be viewed in the online issue, which is available at wileyonlinelibrary.com.]

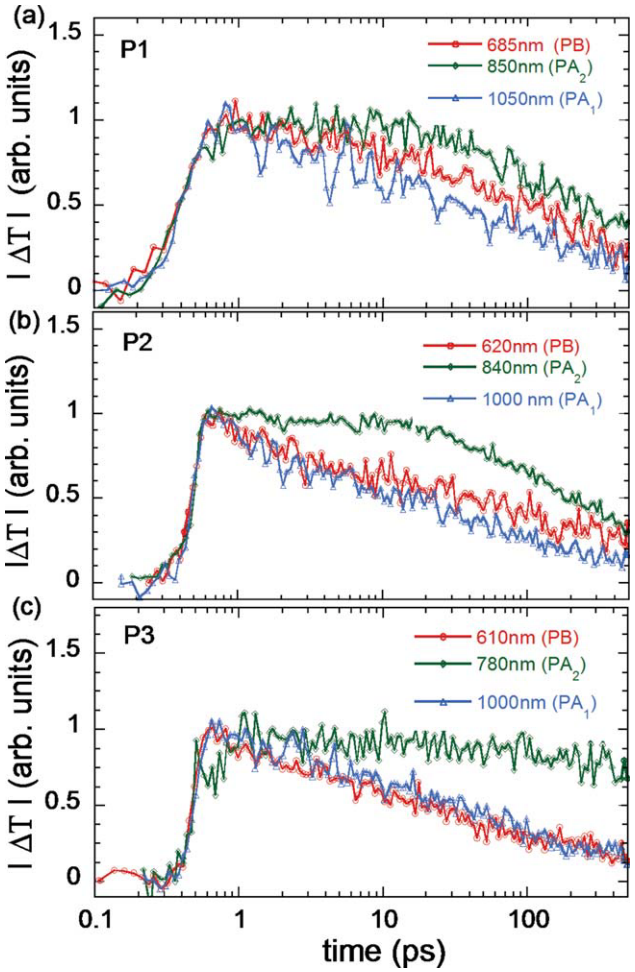

FIGURE 11 Transient dynamics of **P1**, **P2**, and **P3** TA bands. [Color figure can be viewed in the online issue, which is available at wileyonlinelibrary.com.]

The photoexcitations of each sample were characterized more precisely by studying the transient dynamics of three TA bands, as shown in Figure 11. For all three polymers, the decay dynamics of the PA_1 and PB bands were similar, but the bands were clearly separated from the slower PA_2. The dynamics of the PA_2 band showed a time evolution in **P3** that clearly differed from the time evolution in **P1** or **P2**. In **P1** and **P2**, generation of the PA_2 bands occurred within the time resolution of our experimental system (~200 fs), indicating the prompt generation of the polaron pairs. Ultrafast charge generation was attributed to the charge-transfer characteristics of **P1** and **P2**, in which efficient ICT occurred between the donor and acceptor to form intrachain polaron pairs. Prompt charge generation has also been observed in other D–A copolymers.[17,18]

The long-time plateau regions arose from the contributions of intrachain polaron recombination and slow charge pair generation due to dissociation of the singlet exciton. A relatively slow buildup of the PA_2 band was observed within 1 ps in the **P3** thin film, on the same time scale as the decay of the PA_1 signal. This indicated that the polaron pair formed from singlet excitons. The absence of prompt charge generation may be related to less effective ICT in **P3**. The polaron pair in **P3** decayed only slightly during the first 500 ps. The much slower decay of PA_2, when compared with **P1** and **P2**, showed that the polaron pairs in **P3** were more localized. The polarons in **P1** and **P2** were delocalized and more mobile polaron pairs.

Figure 12 shows the transient TA spectra over a broad spectral range, from 2.8 to 0.5 eV, at $t = 1$ ps, following pulse excitation at 400 nm, which excited the higher energy absorption peak of the three polymers. The TA spectra were similar to those produced by excitation at 600 nm (low energy absorption band), shown in Figure 9. The PB band in the higher energy spectra (near the high energy ground state absorption peak) was quite weak, indicating quick internal conversion from the higher excited states to the lowest excited states. The PA_2 bands in **P1** and **P2** were substantially stronger than that in **P3**, showing that polaron pair generation was more efficient in **P1** and **P2** films than in **P3**. We also measured the dynamics of the two PA bands for

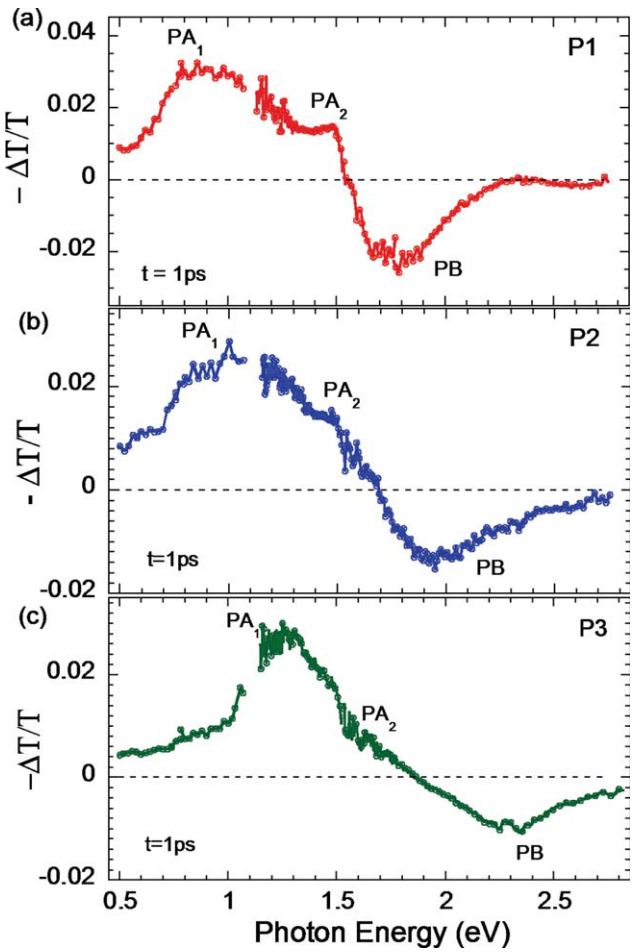

FIGURE 12 The transient TA spectra with broader spectra range from 2.8 to 0.5 eV at $t = 1$ ps. [Color figure can be viewed in the online issue, which is available at wileyonlinelibrary.com.]

each polymer (not shown). The transient dynamics of the PA_1 bands showed similar decay behavior for all three polymers. The PA_2 band indicated prompt charge generation followed by fast decay (<5 ps) in all three polymers when pumped at 400 nm, indicating that the polaron pairs were generated immediately on high energy excitation.[19] It was noted that the peaks of the PA_1 band were blue shifted in moving from **P1** to **P2** to **P3**. The shapes of the PA_1 bands for **P1** and **P2** were very similar. They were much broader than the PA_1 peak in **P3**. The broader PA_1 band in **P1** and **P2** may be related to shifts or splits in the energy levels induced by strong interactions between the donor and acceptor units. Because the stronger PA_2 bands in **P1** and **P2** have wide spectral ranges, they may contribute to the broader PA_1 band, in combination with the contribution from singlet absorption. The higher charge generation efficiency (shown in the TA spectra) and the higher mobility polaron pairs in **P1** and **P2**, relative to **P3**, may explain the higher mobility of the charge carriers in **P1** and **P2** than in **P3** FET measurements.

EXPERIMENTAL

Materials

Synthetic details for the copolymers are described in the Supporting Information.

Sample Preparation for Optical Spectroscopy

All thin film samples for UV–Vis absorption measurements were prepared by spin-coating (3000 rpm, 60s) on quartz substrates using a 1 wt % solution in chlorobenzene. UV–Vis absorption spectra were taken using a Shimadzu UV-2401 PC dual beam spectrometer.

FET Device Fabrication and Characterization

Polymer FETs (with the top contact geometry) were fabricated on heavily doped n-type silicon (Si) wafers each covered with a thermally grown silicon dioxide (SiO_2) layer with thickness of 200 nm. The active layer was deposited by spin-coating at 2500 rpm. Before active layer deposition, SiO_2 surfaces were treated with octyltrichlorosilane (OTS) to make the surfaces hydrophobic. All solutions were prepared at a concentration of 0.5 wt % in chlorobenzene. The thickness of the deposited films was about 70 nm. Before deposition of source–drain electrodes, the films were dried on a hot plate and stabilized at 80 °C for 30 min. All fabrication processes were carried out in a glovebox filled with N_2. Au source and drain electrodes were deposited by thermal evaporation using a shadow mask. The thickness of the source and drain electrodes was 50 nm. The channel length (L) and channel width (W) were 50 μm and 3.45 mm, respectively. Post-thermal annealing processes were carried out on a calibrated and stabilized heat stage (HCS600V, INSTEC) under a N_2 atmosphere. After annealing, the devices were placed on a metal plate at room temperature to cool. Electrical characterization was performed using a Keithley semiconductor parametric analyzer (Keithley 4200) under a N_2 atmosphere.

Sample Preparation for AFM and XRD

Thin film samples for AFM measurements were prepared by spin-coating on a Si wafer covered with 200 nm SiO_2 precoated with OTS using the same solution (0.5 wt % in chlorobenzene) used to prepare the FET devices. AFM images were obtained using a multimode microscope with a Nanoscope controller IIIa (Veeco).

Ultraviolet Photoelectron Spectroscopy

Ultra thin films for UPS measurement were fabricated under a N_2 atmosphere by spin-coating on Au substrates using a 0.1 wt % solution, and the samples were transferred via an airtight sample holder to the UPS analysis chamber. Samples were subsequently kept in a high-vacuum chamber overnight to remove solvent residues. The UPS analysis chamber was equipped with a hemispherical electron energy analyzer (Kratos Ultra Spectrometer) and a UV (He I) source and was maintained at 1×10^{-9} Torr. UPS spectra were collected along a direction normal to the surface with a photon incidence angle of 35°.

Photoexcitation Spectroscopy

The TA spectra were measured using ultrafast pump–probe spectroscopy. The Ti:sapphire laser system with a regenerative amplifier provided 120 fs pulse (1 mJ energy per pulse) at a photon energy of 1.55 eV at a repetition rate of 1 kHz. The pump beam was generated using either the second harmonic of the fundamental emission from the Ti:sapphire laser (3.1 eV) or by an OPA (from 2.25 to 1.8 eV). The probe beam in the visible and near-IR spectral ranges was obtained from a white light supercontinuum spanning 1.6 to 2.8 eV. The white light was generated using a portion of the output from the Ti:sapphire amplifier system and a 1-mm thick sapphire plate. The probe beam in the mid-IR was generated using a difference-frequency method using the signal and idler beams of the OPA. The probe beam was delayed with respect to the pump beam using a computerized translation stage for time delays up to 1 ns.

CONCLUSIONS

We have demonstrated that substitution of alkyl side chains at different positions of a thiophene moiety can affect the optical and electrical properties of D–A conjugated copolymers. The absorption spectra of both **P2** and **P3** tended to blue shift relative to the absorption spectrum of **P1**. A comparison between **P2** and **P3** indicated that the head–head configuration of the substituted alkyl side chain (**P3**) more significantly altered the ICT properties than the tail–tail configuration of the substituted alkyl side chain (**P2**). The electrical transport properties explored in the FETs were more sensitive to the side chain position. The measured mobility of **P2** ($\mu_2 = 1.8 \times 10^{-3}$ cm^2/V s) was slightly lower than that of **P1** ($\mu_1 = 4.9 \times 10^{-3}$ cm^2/V s). However for **P3**, the measured mobility was very low ($\mu_3 = 3.8 \times 10^{-6}$ cm^2/V s).

Semiempirical quantum chemical calculations showed that the charge-density isosurfaces of the HOMO levels of **P1** and **P2** were delocalized over both the donor and acceptor sites.

However in **P3**, the structure of the conjugated backbone was dramatically twisted, and both the LUMO and HOMO orbitals were localized due to strong steric hindrance by the alkyl side chains in the head–head configuration.

Photoexcitation spectroscopy showed higher charge generation efficiencies (shown in the TA spectra) and higher mobility polaron pairs in **P1** and **P2** than in **P3**. Therefore, we attributed the poor device performance of **P3** to low charge generation efficiency and charge localization occurred by large steric hindrance.

Substituted side chains critically affected the optical and electronic properties of D–A conjugated copolymers. Although the substituted side chains provided better solubility for the D–A conjugated copolymers, the intrinsic polymer properties were significantly altered due to disturbance of ICT between the donor and acceptor segments. Furthermore, the position of the side chain was very important for controlling the optical and electrical properties of the D–A conjugated copolymers.

This work was supported by Priority Research Centers Program through the National Research Foundation of Korea (NRF) funded by the Minstery of Education, Science and Technology (2009-0093818). This study in University of California at Santa Barbara was supported by the Global Research Project (Grant No. SB080019) and by the Heeger Center for Advanced Materials at the Gwangju Institute of Science and Technology (GIST). This study in Korea Research Institute of Chemical Technology was supported by a grant (M2009010025) from the Fundamental R&D Program for Core Technology of Materials funded by the Ministry of Knowledge Economy (MKE) and by the Korea Energy Management Corporation (KEMCO) under the New and Renewable Energy R&D Grant (2008-N-PV08-02), Republic of Korea.

REFERENCES AND NOTES

1 Svensson, M.; Zhang, F.; Veenstra, S. C.; Verhees, W. J. H.; Hummelen, J. C.; Kroon, J. M.; Inganäs, O.; Andersson, M. R. Adv Mater 2003, 15, 988–991.

2 Blouin, N.; Michaud, A.; Gendron, D.; Wakim, S.; Blair, E.; Neagu-Plesu, R.; Belletête, M.; Durocher, G.; Tao, Y.; Leclerc, M. J Am Chem Soc 2008, 130, 732–742.

3 Blouin, N.; Michaud, A.; Leclerc, M. Adv Mater 2007, 19, 2295–2300.

4 Scharber, M. C.; Mühlbacher, D.; Koppe, M.; Denk, P.; Waldauf, C.; Heeger, A. J.; Brabec, C. J Adv Mater 2006, 18, 789–794.

5 Wang, E.; Wang, L.; Lan, L.; Luo, C.; Zhuang, W.; Peng, J.; Cao, Y. Appl Phys Lett 2008, 92, 033307.

6 Kline, R. J.; McGehee, M. D.; Kadnikova, E. N.; Liu, J.; Fréchet, J. M. J. Adv Mater 2003, 15, 1519–1522.

7 Zen, A.; Pfluam, J.; Hirschmann, S.; Zhuang, W.; Jaiser, F.; Asawapirom, U.; Rabe, J. P.; Schref, U.; Neher, D. Adv Funct Mater 2004, 14, 757–764.

8 Roncali, J.; Macromol Rapid Commun 2007, 28, 1761–1775.

9 Jayakannan, M.; Van Hal, P. A.; Janssen, R. A. J. J Polym Sci A: Polym Chem 2002, 40, 251–261.

10 Cho, S.; Seo, J. H.; Kim, S. H.; Song, S.; Jin, Y.; Lee, K.; Suh, H.; Heeger, A. J. Appl Phys Lett 2008, 93, 263301.

11 Moulé, A. J.; Tsami, A.; Bünnagel, T. W.; Forster, M.; Kronenberg, N. M.; Scharber, M.; Koppe, M.; Morana, M.; Brabec, C. J.; Meerholz, K.; Scherf, U. Chem Mater 2008, 22, 4045–4050.

12 Gadisa, A.; Mammo, W.; Andersson, L. M.; Admassie, S.; Zhang, F.; Andersson, M. R.; Inganäs, O. Adv Funct Mater 2007, 17, 3836–3842.

13 Jespersen, K. G.; Beenken, W. J. D.; Zaushitsyn, Y.; Yartsev, A.; Andersson, M.; Pullerits, T.; Sundström, V. J. Chem Phys 2004, 121, 12613–12617.

14 Perzon, E.; Wang, X.; Admassie, S.; Inganäs, O.; Andersson, M. R. Polymer 2006, 47, 4261–4268.

15 Salaneck, W. R.; Lögdfund, M.; Fahlman, M.; Gresinski, G.; Kugler, Th. Mater Sci Eng 2001, R34, 121–146.

16 Westerling, M.; Aarnio, H.; Osterbacka, R.; Stubb, H.; King, S. M.; Monkman, A. P.; Andersson, M. R.; Jespersen, K.; Kesti, T.; Yartsev, A.; Sundstrom, V. Phys Rev B 2007, 75, 224306.

17 Kraabel, B.; Klimov, V. I.; Kohlman, R.; Xu, S.; Wang, H.-L.; McBranch, D. W. Phys Rev B 2000, 61, 8501–8515.

18 Pacios, R.; Nelson, J.; Bradley, D. D. C.; Virgili, T.; Lanzani, G.; Brabec, C. J. J Phys Condens Matter 2004, 16, 8105–8116.

19 Arkhipov, V. I.; Emelianova, E. V.; Bassler, H. Phys Rev Lett 1999, 82, 1321–1324.